Solar Phys (2007) 241: 53–66
DOI 10.1007/s11207-007-0251-5

Spectral Diagnostics of the Magnetic Field Orientation in a Prominence Observed with SOHO/SUMER

B. Schmieder · S. Gunár · P. Heinzel · U. Anzer

Received: 29 June 2006 / Accepted: 19 January 2007 /
Published online: 14 March 2007

Abstract During several campaigns focused on prominences we have obtained coordinated spectral observations from the ground and from space. The SOHO/SUMER spectrometer allows us to observe, among others, the whole Lyman series of hydrogen, while the Hα line was observed by the MSDP spectrograph at the VTT. For the Lyman lines, non-LTE radiative-transfer computations have shown the importance of the optical thickness of the prominence – corona transition region (PCTR) and its relation to the magnetic field orientation for the explanation of the observed line profiles. Moreover, Heinzel, Anzer, and Gunár (2005, *Astron. Astrophys.* **442**, 331) developed a 2D magnetostatic model of prominence fine structures that demonstrates how the shapes of Lyman lines vary, depending on the orientation of the magnetic field with respect to the line of sight. To support this result observationally, we focus here on a round-shaped filament observed during three days as it was crossing the limb. The Lyman profiles observed on the limb are different from day to day. We interpret these differences as being due to the change of orientation of the prominence axis (and therefore the magnetic field direction) with respect to the line of sight. The Lyman lines are more reversed if the line of sight is across the prominence axis as compared to the case when it is aligned along its axis.

Keywords Prominences · Hydrogen Lyman lines · Solar magnetic fields

B. Schmieder (✉)
Observatoire de Paris, Laboratoire d'Etudes Spatiales et d'Instrumentation en Astrophysique, 92195 Meudon Cedex, France
e-mail: brigitte.schmieder@obspm.fr

S. Gunár · P. Heinzel
Astronomical Institute, 25165 Ondrejov, Czech Republic

S. Gunár
Astronomical Institute, Faculty of Mathematics and Physics, Charles University, Prague, Czech Republic

U. Anzer
Max-Planck-Institut f. Astrophysik, Karl-Schwarzschild Str. 1, 85740 Garching, Germany

1. Introduction

Solar prominences consist of cool plasma located in the hot corona and supported against gravity by external forces, either of dynamic or magnetic nature. The dynamic models invoke injection of chromospheric plasma from below. The injection can be produced by thermal instability, leading to dynamic condensation along flux tubes (Poland and Mariska, 1986; Karpen, Antiochos, and Klimchuk, 2006), by Alfvén waves (Lin, 2002) or by reconnection-driven flows (Litvinenko and Martin, 1999).

Magnetic hydrostatic models for quiescent prominences were first proposed in 1D by Kippenhahn and Schlüter (1957) and Kuperus and Raadu (1974). The prominence as a whole is represented by dipped magnetic field lines in a vertical plane. A straightforward generalisation of these models to fine structures can be envisioned as purely local magnetohydrostatic (MHS) equilibria, producing many local magnetic dips everywhere. Such a scenario was first proposed by Poland and Mariska (1988), who considered local magnetic dips due to the cool plasma weight. These dips would propagate vertically to form apparent narrow vertical plasma threads. Heinzel and Anzer (2001) developed this solution of 2D MHS equilibria coupled to non-LTE radiative transfer in two dimensions. In 3D approaches, MHS modelling using linear or nonlinear force-free fields was recently studied by different groups, who showed that prominence fine structures could be mapped by dips of magnetic arcades computed by extrapolation using photospheric magnetograms as boundary conditions (Aulanier and Démoulin, 1998; Aulanier and Schmieder, 2002; van Ballegooijen, 2004; Régnier and Amari, 2004).

The observations of prominences require long exposure times (∼3 times longer than for filaments) and generally it is difficult to distinguish the fine structures even with high-resolution telescopes and thus to define physical quantities of the fine structures, *i.e.* magnetic field, velocity field and optical thickness. However, at the limb it is possible to have good diagnostics to define the orientation of prominence fine threads and their physical parameters.

In this paper we propose two methods to derive the orientation of the magnetic field in prominences. The first one is purely a morphological analysis when the filament is first observed on the disk. The second uses the hydrogen Lyman line series for diagnostics as recently proposed in theoretical work based on the thickness of the prominence – corona transition region (PCTR) (Heinzel and Anzer, 2001; Heinzel, Anzer, and Gunár, 2005).

The thickness of the PCTR is interpreted in terms of the integration along or across the field lines. The reversed profiles were assigned to a prominence viewed across the field lines (narrow PCTR), while the unreversed ones belong to a prominence viewed along field lines where the PCTR is assumed to be much more extended. Therefore, the line profiles should be different for observations of prominences along their axis or perpendicular to it.

The prominence that we choose to use for this study presents a round-shaped structure when observed on the disk. Thus the fine structures of this filaments appear on the limb obviously with different orientations. In Section 2 we present the morphological diagnostics leading to an empirical determination of the orientation of the fine structures and therefore of the magnetic field. In Section 3 the Lyman line profiles observed by SOHO/SUMER (Wilhelm *et al.*, 1995) are presented and discussed in the frame of the theoretical models of Heinzel, Anzer, and Gunár (2005).

We conclude that the results of the two methods are in agreement and thus the Lyman lines are good diagnostics to derive the orientation of the magnetic field and the physical parameters of the fine structures.

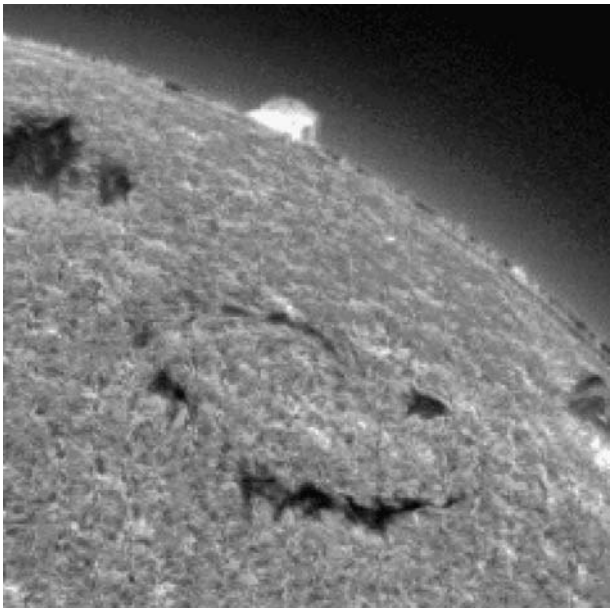

Figure 1 BBSO observation of a round-shaped filament on the disk on October 12, 1999, at 14:04 UT. The field of view is 420 × 420 arcsecs. The orientation of its fine structures indicates that it is a dextral filament.

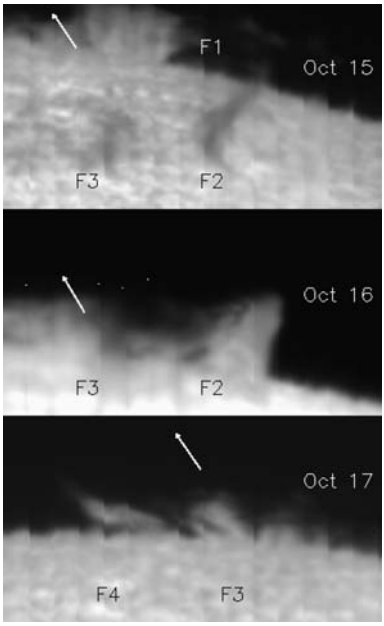

Figure 2 Prominences observed on October 15 at 11:45 UT, on October 16 at 11:37 UT and on October 17, 1999, at 11:37 UT with the MSDP at the VTT. The letters F2, F3 and F4 indicate the latitude positions of different sections of the round filament. On October 15, the sections F2 and F3 are on the disk; they cross the limb on the next day and erupt on October 17. The arrows indicate the North direction and approximately the direction of the SUMER slit. The SUMER slit (120 arcsecs long) crosses the limb and the prominence. The field of view is 228 × 100 arcsecs.

2. Observations of the Filament

2.1. Overview

The filament/prominence used for this study was observed from October 15 to 17, 1999 (N45° – 55°, W50° – 90°), as a target of the MEDOC coordinated campaign between SOHO

and ground-based instruments. A filament with a round shape was observed during three days before crossing the limb (Figure 1). We concentrate our study on the observations obtained mainly with the SUMER spectrometer (Wilhelm *et al.*, 1995) and in addition we used the observations made with the Multi-channel Subtractive Double Pass spectrograph (MSDP) (Mein, 2002) operating on the German solar telescope VTT in Tenerife (Table 1). The VTT has no pointing information; only approximative coordinates can be derived from comparison with synoptic full-disk observations. The VTT observations are presented in Figure 2 and synoptic data in Figure 3. In Meudon spectroheliograms, a SOHO/EIT image at 304 Å and high-contrast spectroheliograms of Big Bear Solar Observatory (BBSO) we see that the round-shaped filament consists of four sections (F1, F2, F3 and F4) that successively cross the limb. The analysis of the filament will allow us to have a 3D view of the fine structures of the prominence.

2.2. Morphological Diagnostics of the Orientation of the Prominence Fine Structures

The fine structures of filaments observed on the disk with high spatial resolution can indicate the orientation angle θ of the horizontal component of the magnetic field versus the filament axis because the magnetic field lines are frozen in the plasma. In our case the round-shaped filament is observed on the disk with survey instruments having a relatively low resolution (Figure 1); therefore, the fine structures are not really visible. We see mainly the barbs and the orientation of their axis, which indicates the chirality of the filament (which is dextral in our case according to the criteria of Martin, 1998) but not really the orientation of the fibrils.

Observationally, the orientation angle of the horizontal magnetic vector with respect to the prominence axis has been statistically measured by Leroy, Bommier, and Sahal-Bréchot (1984). From 256 observed prominences, they found a value of $\theta = -25°$ with a large uncertainty. This uncertainty reflects the dispersion of the 256 measurements, one for each prominence.

A recent study of models based on three-dimensional constant-α (linear) magneto-hydrostatic (MHS) extrapolations of observed photospheric line-of-sight magnetograms gives us new insight on the different characteristics of the magnetic field in prominences (Aulanier and Démoulin, 2003). In particular, it is shown that the θ angle is commonly constant in each prominence and lower than $-20°$ for altitudes larger than few Mm, which correspond to the main body of prominences. On the other hand, at lower altitudes the values of θ may have a larger dispersion. For a given prominence these dispersed values could correspond to fine structures in feet or barbs. In this study we consider mainly the body of the prominence and assume a small θ angle. This seems reasonable in our case. Thus we can deduce the orientation of the prominence versus the line of sight:

- If the main axis of a filament is oriented along a solar meridian (North – South orientation), the fine structures are also more or less oriented along the meridian.
- If the filament axis follows a parallel to the equator, the fine structures are also more or less oriented East – West.
- Viewed at the limb, a filament oriented North – South will appear as an arch, the barbs being the footpoints of the arch. We can say that the line of sight is crossing the magnetic fine structures.
- A filament oriented East – West will appear as a compact prominence, with all its main axis integrated along the line of sight. In that case the line of sight follows the main direction of the magnetic field of the structures.

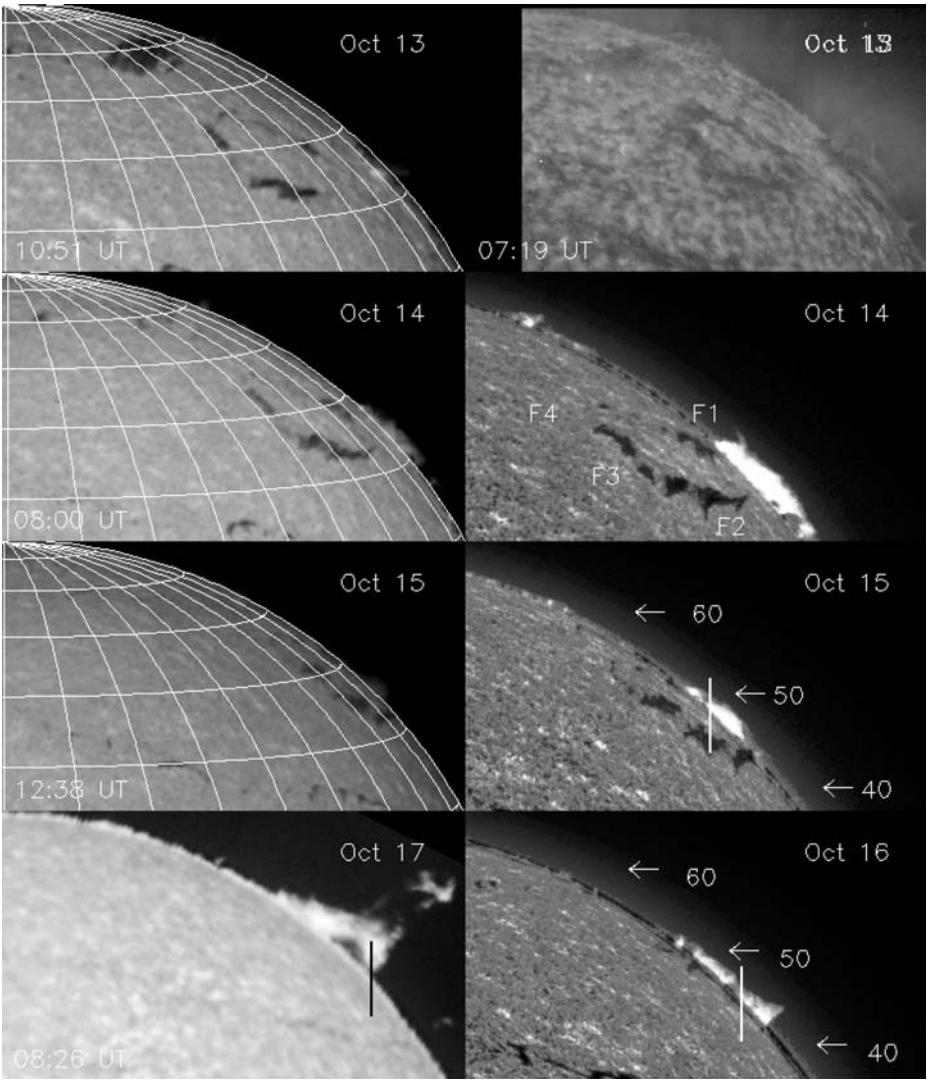

Figure 3 Observations of a round-shaped filament/prominence (F1, F2, F3, F4) from October 13 to October 17, 1999: in the left column, prominence at Meudon Hα spectroheliograms with superposed heliographic coordinates grid for October 13, 14 and 15 (rows 1, 2 and 3); in the right column are presented one observation with SOHO/EIT at 304 Å at 07:19 UT (top panel) and the BBSO observations in Hα obtained around 15 UT. Notice the round-shaped channel in the He II 304 Å EIT image. In the last row, the right panel is the BBSO image for October 16 and the left panel is the Meudon Hα image with the eruptive prominence on October 17 at 08:26 UT. The vertical line in the prominences observed on October 15, 16 and 17 represents the approximate location of the SUMER slit for the time series observations. The arrows, followed by numbers, indicate the latitudes N40°, N50° and N60°.

This discussion allows us to derive from filament observations the orientation of the fine structures versus latitude and longitude and finally versus the line of sight. The round-shaped filament that we have observed during three days consists of several sections (F1, F2, F3 and F4) well visible on October 14 before it crosses the limb (Figure 3). Sections F1 and F3 are

Table 1 Coordinates of the prominence observations with SOHO/SUMER and the VTT telescope. (Column 2: x, y are the coordinates of the centre of the SUMER slit in arcseconds, column 3: their corresponding heliographic latitudes, column 4: times of the observations at the VTT, column 5: intervals of the time series observed with SUMER.)

Date	x, y [arcsecs]	Latitude [degrees]	VTT [UT]	SUMER [UT]
15 Oct	634, 743	N50	11:45, 16:21	13:45 – 15:10
16 Oct	682, 675	N45	11:37, 12:30, 16:30	11:35 – 14:58
17 Oct	654, 716	N48	11:37, 14:30, 16:30	11:31 – 14:54

oriented North – South; Sections F2 and F4 are oriented East – West. The prominence on October 15 is formed by section F1 located at N50° (Figure 3). The line of sight is crossing the fine structures. On October 16 the prominence consists of two sections, with the southern part (located at N45°), section F2, crossing the limb (Figure 3). The fine structures are integrated along the line of sight, which follows more or less the direction of the magnetic field. In contrast, the northern part of the prominence between N50° and N60° is section F3, oriented North – South, and we could expect that the line of sight is perpendicular to the fine structure axis (or the magnetic field direction). This is in agreement with the North – South orientation of the barbs, which are easily visible on October 12 (Figure 1). On October 17 the prominence should correspond to the top of sections F3 and F4. The prominence is eruptive at 08:26 UT (Figure 3), still visible on the VTT observation at 11:37 UT (Figure 2) and gone in the BBSO image at 15:10 UT. The structures should be integrated along the line of sight.

The heliographic coordinates (latitude and longitude) of the different sections of the filament when crossing the limb are extrapolated and for each day we see which section appears as a prominence. We propose an approximate value of the angle ϕ between the line of sight and the fine structures of the different sections as they are observed over the limb by SUMER in order to summarise the previous discussion (Table 2).

This method is empirical and thus uncertain. We have to assume that no drastic changes occur in the filament before crossing the limb and that the fine structures have the same orientation as the filament axis. Even though this looks reasonable for our round-shaped filament it could be still questionable according to recent observations of filaments with high spatial resolution (O. Engvold, private communication). In the next section we present a second diagnostic method to derive the orientation of the prominence based on the shape of the Lyman lines.

3. Lyman Lines

3.1. SUMER Observations

The Joint Observing Program JOP 107 was running using the CDS and SUMER spectrometers. However, in this study we did not use the CDS observations. The main characteristics of the observation sequences with SUMER are presented in Table 3. We will name the Lyman lines as follows: L2 for Lyman β, L3 for Lyman γ, L4 for Lyman δ and so on. SUMER observed time series of the Lyman lines using two wavelength ranges, one centred on L2 and

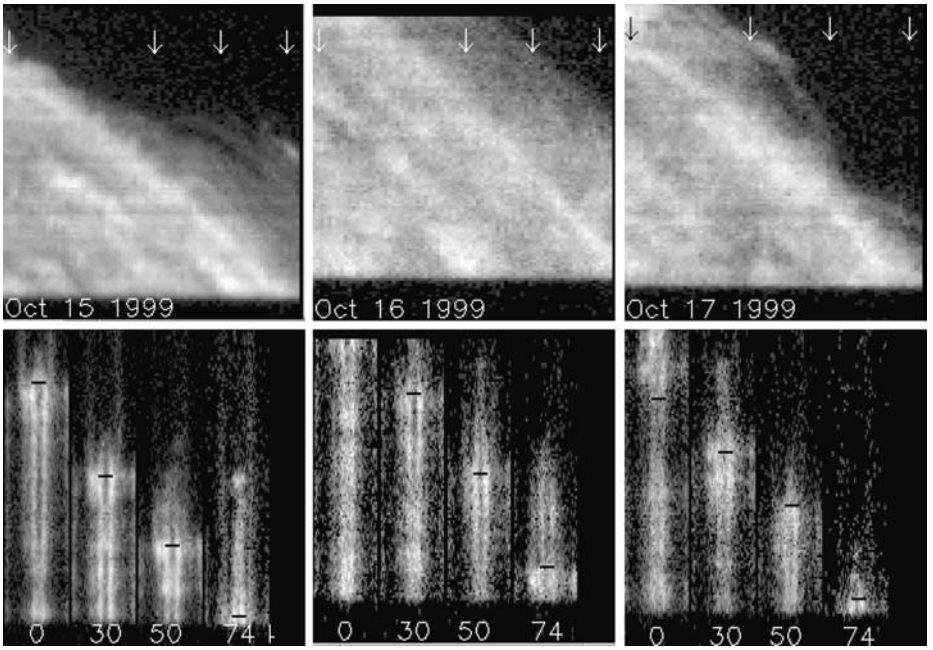

Figure 4 Rasters made with SUMER time series of 76 spectra in the L4 line through the prominences on October 15 at 13:45 UT, October 16 at 11:35 UT and October 17 at 11:31 UT (during 40 min). The field of view of the images is about 114 × 110 arcsecs (approximatively 10 degrees in latitude). Some spectra (110 arcsecs in the *y* direction) are presented below; their positions are indicated by numbers and arrows in the images. The limb is identified by brightenings and is indicated by black horizontal lines over the spectra. Some data are missing at the bottom of the spectra and for October 16 also at the top (black areas). North is up.

Table 2 Heliographic positions in degrees (latitude N and longitude W) of sections F1, F3 and F4 of the filament measured on the grid over the spectroheliograms and then extrapolated as the filament is crossing the limb; ϕ is the approximate value of the angle between the line of sight and the fine structures at the limb derived with the morphological diagnostics. The asterisks indicate the sections observed by SUMER on October 15, 16 and 17, respectively.

Section	Day Latitude	12 W	13 W	14 W	15 W	16 W	17 W	ϕ [degrees]
F1	N50	50	62	75	88*			90°
F2	N45		40 – 55	53 – 70	70 – 80	83 – 93*		0°
F3	N45 – 55	28	40	52	70	83*		90°
F4	N50	28	44	57	68	81	94*	0°

the other one on the higher lines in the series (L4 and L5 to L10). Full spectra (40 Å) were registered for wavelength calibration. Context rasters were performed in the L4 (949.74 Å) and SVI (944.54 Å) lines by scanning the region of the filament/prominence at the beginning and end of the sequences of observations with a step of 1.5 arcsecs covering a field of view of 114 × 120 arcsecs with 76 spectra obtained in 40 min. These two modes were followed

Table 3 Characteristics of the SUMER program (JOP107). The sequence of observations is repeated several times during the observing periods. The program starts and ends with "rastering" the region in L4 and S VI lines (Figure 4); "full spectra" means that 40 Å spectra covering the detector is registered; "7 or 2 lines" means that only 7 or 2 short spectra centred on 7 or 2 lines are registered.

Mode	Lines	Number of windows	Cadence	Exp. time [sec]	Duration [min]	Slit
Raster	L4, S VI	2	76	30	40	4/7
Full spectra	L4 – L10	1	1	127	2	5/8
7 lines	L4 – L7, S VI, O IV	7	16	45	12	5/8
2 lines	L2, O VI	2	2	30	2	5/8
...						
Raster	L4, S VI	2	76	30	40	4/7

by time series of spectra centred on 7 lines or 2 according to the wavelength range (using 7 or 2 windows over the detector to gain time and telemetry space). The observations were performed by using the 1 × 120 arcsec slit (slit 4/5) on October 15 and the 0.3 × 120 arcsec slit (slit 7/8) for October 15, 16 and 17. Slits 4 and 7 are centred on the detector; slits 5 and 8 are positioned in the low part of the detector. In fact 10 pixels in the North – South direction are not available and therefore the size of the images are 115 by 110 arcsecs. Figure 4 shows images of the prominences and parts of the disk obtained from the rastering mode in the L4 line by integrating the line profiles. The limb appears brighter than the disk. The raster frames correspond to a total dimension 114 × 120 arcsecs but because of bad pixels the images are reduced to 114 × 110 arcsecs. Below each raster we present, as examples, four spectra showing large reversed profiles on the disk, similar to filament profiles that we have studied in previous papers, and weak reversed and unreversed profiles for the prominences. Some sections of the spectra in the bottom and at the top are black because of missing data. On October 15, L4 is weak in the prominence and the profile is reversed except in the spectra corresponding to the right side of the raster where the prominence is brighter with some ejected bubbles (spectra 74). On October 16 all the profiles are reversed while on October 17 they are mainly not reversed.

3.2. Lyman Line Profiles

The L2 line spectra for the three days (October 15 – 17) are presented in Figure 5. The location of these spectra corresponds to the central part of the raster in Figure 4. Detached blobs of material are visible from time to time. It is not possible to accurately determine the position of the SUMER slit in the prominence, since the coordinates indicated in the header of the files are not always correct. Besides, the spectra have a curved shape and spatial co-alignment between L2 and L4 spectra needs a shift of 5 pixels in the direction of the slit. L2 gives a different co-alignment than L4. Using the SUMER raster we co-align the L4 observation with the Hα observation obtained with the VTT. Figure 2 shows the prominence observed with the MSDP on the VTT and the arrows indicate roughly the SUMER slit direction. The slit crosses the limb and the prominences. On October 15, the slit of SUMER crosses the F1 fine structures, on October 16, it crosses the F3 fine structures and on October 17 the slit integrates the F3 – F4 structures while the prominence is erupting.

The integrated intensities of the Lyman lines in the prominences are summarised in Table 4; they are relatively low compared with the intensities of the observed prominences

Table 4 Integrated intensities of Lyman lines observed on the disk (disk) and in prominences (prom) in erg/s/cm^2/sr. The pixel number indicates the interval in pixels along the slit where mean prominence profiles were calculated (approximatively 10 to 20 arcsecs long).

Date	Pixels	L2 disk	L2 prom	L4 disk	L4 prom	L5 disk	L5 prom
15 Oct	41 – 50	996	158	140	40	79	17
16 Oct	20 – 30	1194	187	155	33	96	23
	5 – 20	719	159	88	20	66	17
17 Oct	35 – 45	891	164		11	15 – 22	7.4

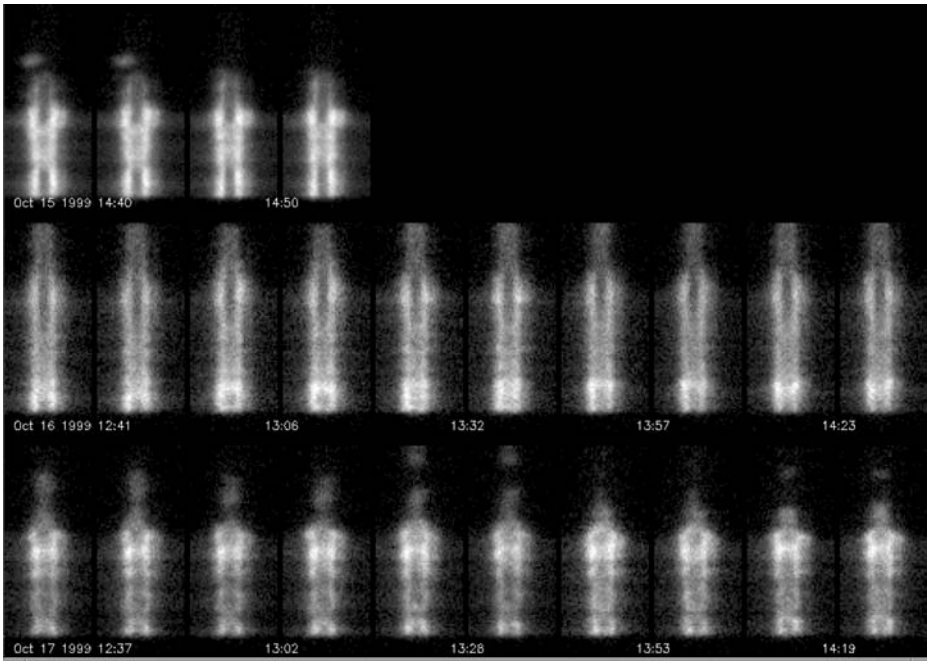

Figure 5 Temporal changes in the spectra of L2 observed partly on the disk and partly in the prominence (the limit between the disk and the prominence can be identified by its increased brightness): top panels on October 15, 1999 (the profiles are strongly reversed; notice a bubble at the top of the prominence with large velocities at 14:40 – 41 UT); middle panels on October 16 between 12:42 and 14:23 UT (the profiles are reversed); bottom panels on October 17 between 12:37 and 14:19 UT. Notice that the profiles are in emission in the prominence and that detached blobs of material are visible from time to time, particularly on October 17, as the prominence is erupting. The profiles on the disk are all reversed; they should correspond to filaments before crossing the limb.

presented by Heinzel *et al.* (2001). This round-shaped filament leads to a rather weak prominence.

Figure 6 shows typical examples of Lyman line profiles (L2, L4, L5, L6 and L7) for the three days. The characteristics of the Lyman lines "reversed or not reversed" depends on the prominence but not on the Lyman line in the series.

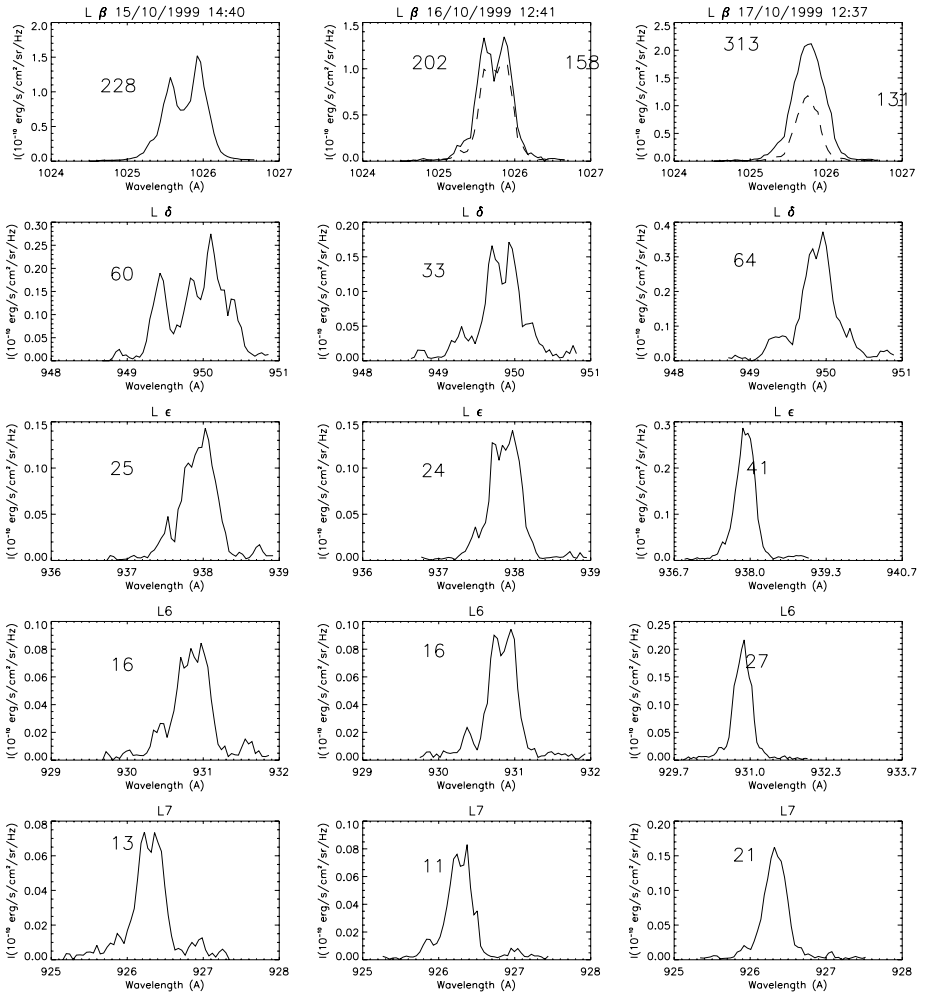

Figure 6 Examples of L2 (Lβ), L4, L5, L6 and L7 profiles in the prominences averaged over a few pixels along the slit to reduce noise (15 to 20 arcsecs) (continuous line) and a blob (dashed line) observed on October 15, 16 and 17, 1999. On October 15 the He II line in the wing of L4 is very strong (a position of the He II line at the edge of the bare part of the detector could explain such an enhancement). The numbers indicated in each panel correspond to the integrated intensity values (in cgs units).

3.3. Theoretical Lyman-Line Profiles

In our previous works (Heinzel, Schmieder, and Vial, 1997; Schmieder *et al.*, 1998; Heinzel *et al.*, 2001; Schmieder, Tziotziou, and Heinzel, 2003) we have demonstrated the importance of the prominence – corona transition region (PCTR) for the formation of hydrogen Lyman lines. In the case of prominences, the SUMER spectra of two different prominences were explained by two quite different PCTRs modelled in a 1D slab geometry (Heinzel *et al.*, 2001). More consistent models of vertical threads with 2D MHS equilibrium in the horizontal plane were recently introduced by Heinzel and Anzer (2001) and Heinzel, Anzer, and Gunár (2005) (see also Heinzel and Anzer, 2006). Multilevel non-LTE

calculations based on such 2D models clearly show that the computed Lyman-line profiles of prominences strongly depend on the viewing angle with respect to the magnetic-field orientation. The field orientation has a two-fold effect on the Lyman-line shapes. First, the density distribution along the field lines is governed by MHS equilibrium, while across the field lines the gas pressure can vary in a rather arbitrary way because the individual flux tubes are magnetically separated. Second, along the field lines the temperature variation is supposed to be relatively smooth because of efficient heat conduction. On the other hand, heat conduction across the field lines is strongly inhibited, which leads to a steep temperature gradient within the corresponding PCTR.

From the grid of 2D models computed by Heinzel, Anzer, and Gunár (2005) one can conclude that the profiles of Lyman lines higher than Lα are much more reversed when we look across the magnetic field lines. This is opposite to the situation when viewing along the field lines where the Lyman lines, and in particular higher series members, are frequently unreversed. A detailed explanation of this behaviour is given in the previously mentioned paper where various examples are shown for 18 different models.

We used this grid of models to compare theoretical Lyman profiles with the observed ones. Our aim was to find models with profiles similar to those we observed and thus qualitatively derive some parameters of the observed prominence (Figure 4). We concentrated on the L4 line profiles from rasters observed on October 16 and October 17 since we can get better averaged profiles with more points in prominences. We have not used the L4 lines from the raster observed on October 15 since they are blended by the He II line. The spectra of the prominences of each day are well characterised with or without reversal (see Section 3.1). Figures 7 and 8 show the variation of the L4 line along the raster. Each profile of surface plots represents an averaged profile along the slit at a given position on the raster, while plots on the right-hand side are averaged profiles over all raster positions. The averaged profiles keep the characteristics of the individual profile of each prominence while reducing noise.

According to our morphological study (Section 2.2), the filament section F3 is observed as a prominence on October 16. The angle ϕ of the line of sight with the fine structure (magnetic field lines) is approximately 90° (Table 2). On October 17 section F4 is observed with the angle between fine structure and line of sight estimated as 0° (Table 2). Reversed profiles correspond to the fine structure observed across the field, while emission profiles correspond to observations along the field lines. This is in agreement with the predictions of Heinzel, Anzer, and Gunár (2005) models.

3.4. Characteristics of the Models

Within the grid of 18 models we have found those with closest agreement between theoretical and observed L4 lines. Figure 9 shows the L4 profiles of models $\boldsymbol{C}_2$ and $\boldsymbol{C}_4$. In one case the profile represents the averaged profile of the central part of the modelled prominence thread seen across the field ($\boldsymbol{C}_2$). The other profile represents averaged profiles over the width of the thread (1000 km) seen along the field lines ($\boldsymbol{C}_4$). Note that synthetic profiles are chosen as best matches from the grid of models.

Figure 10 shows the temperature variation across the field with two thin PCTR regions with a very steep gradient of the temperature, the density variation across the field (along the width of the thread) and the optical depth variation across the field lines at 949.74 Å.

Figure 11 shows the temperature variation along the field lines with two thicker PCTR regions with a gentle gradient of the temperature, the density variation along the field (along the length of the thread) and the optical depth variation across the field lines at 949.74 Å.

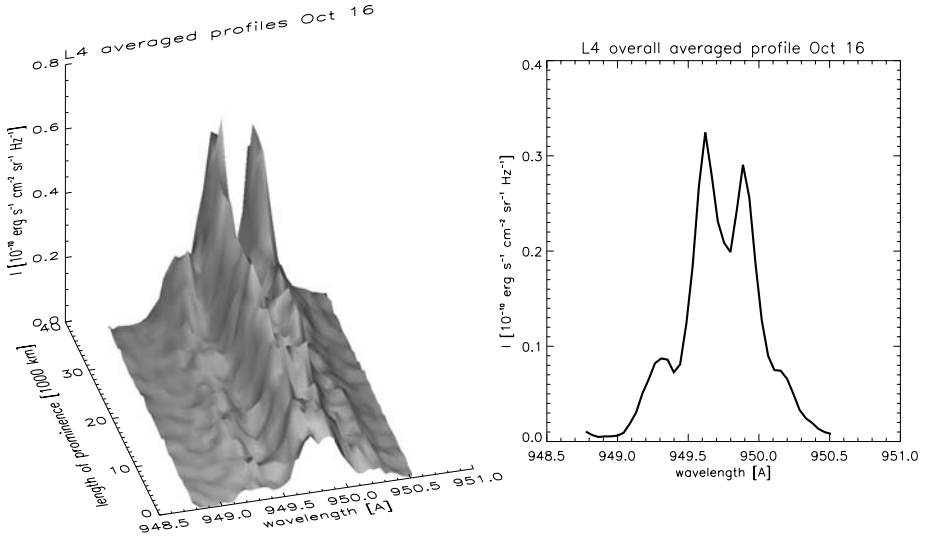

Figure 7 L4 observed on October 16. Surface plot on the left shows the line variation along the raster. Each profile represents an averaged profile along the slit at the given position on the raster. On the right is shown the overall averaged profile along the raster positions.

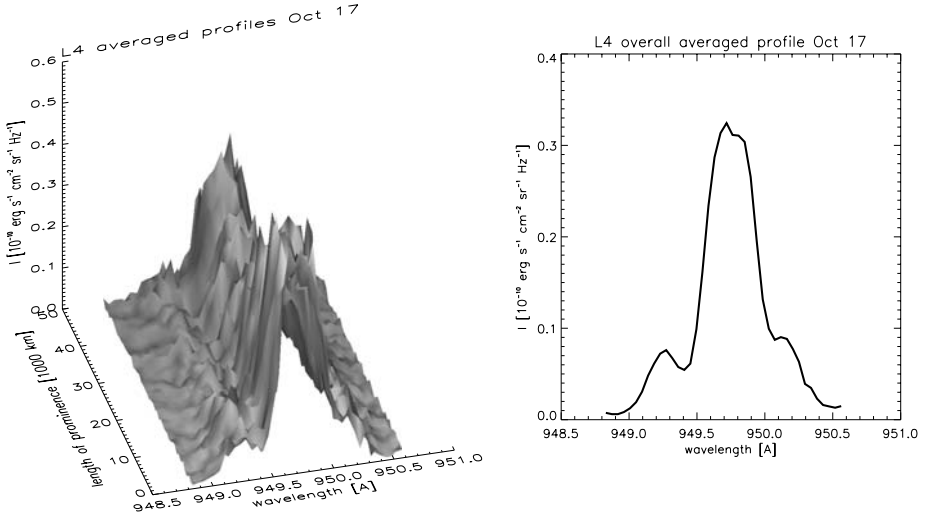

Figure 8 L4 observed on October 17. Surface plot on the left shows the line variation along the raster. Each profile represents an averaged profile along the slit at the given position on the raster. On the right is shown the overall averaged profile along the raster positions.

4. Conclusions

During a MEDOC campaign operated in Orsay, we have observed with the SOHO/SUMER spectrometer a filament crossing the limb on October 15 – 17, 1999. The filament has a

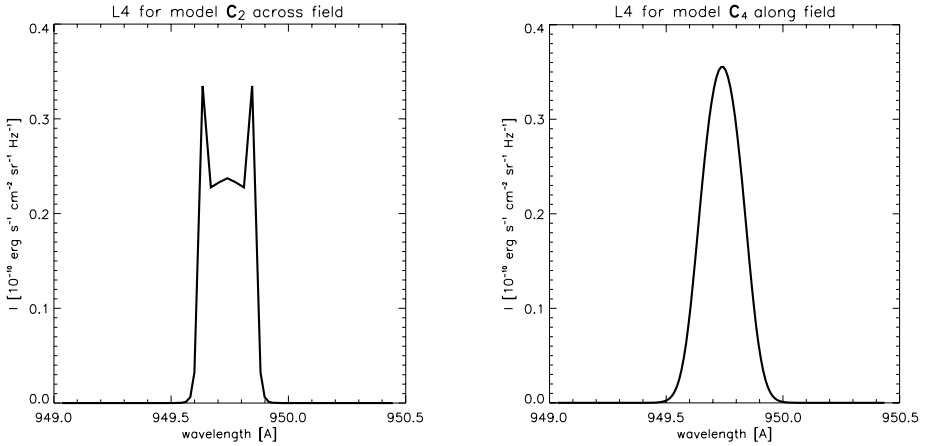

Figure 9 Lyman δ profiles of models $\boldsymbol{C}_2$ (left) and $\boldsymbol{C}_4$ (right).

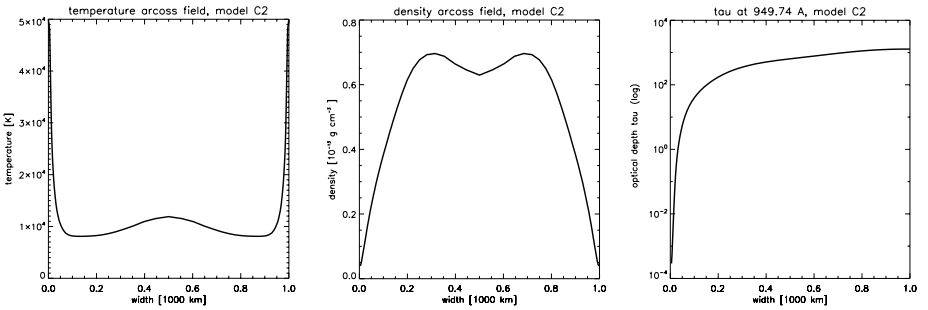

Figure 10 Temperature, density and optical depth variation across the field lines for model $\boldsymbol{C}_2$.

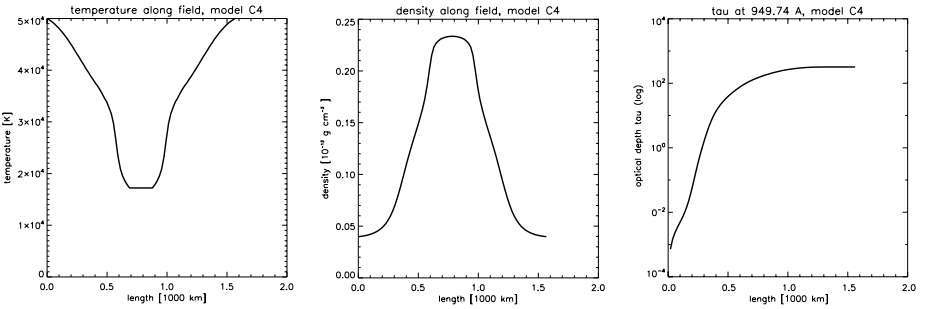

Figure 11 Temperature, density and optical depth variation along the field lines for model $\boldsymbol{C}_4$.

round shape when viewed on the disk and consequently consists of different sections with different orientations. In a first study we use the characteristics of filaments to proceed to a morphological analysis of the different sections and determine the predicted angle between the line of sight and the orientation of the filament, and thus of the magnetic field, as it

crosses the limb and becomes a prominence. In a second part of the work we study the profiles of the Lyman line series observed in the prominences and use the behaviour of the profiles as a diagnostics of the orientation of the magnetic field of the fine structure of the prominences.

The round-shaped filament gives us a unique opportunity to compare the observed Lyman-line profiles (see Figure 6) with theoretical ones. We clearly see how the shape of profiles changes during the subsequent three days when the orientation of the magnetic field with respect to the line of sight is also changed as we derive in this paper. These variations have the same qualitative behaviour as those computed theoretically for 2D thread models. The Lyman lines are more reversed if the line of sight is across the prominence axis as compared to the case when it is aligned along its axis. This result supports the idea that the PCTR can be quite different for different field orientations and that the shape of the Lyman lines provides useful diagnostics for that.

Acknowledgements The authors thank the planners of SOHO instruments during the MEDOC campaign (JOP107). SOHO is an ESA/NASA space mission. This work was done in the framework of the RTN programme (European Solar Magnetism Network, Contract No. HPRN-CT-2002-00313). It was also supported by the ESA-PECS Project No. 98030 and by Grant No. A3003203 of the Grant Agency of the Academy of Sciences of the Czech Republic. BS thanks the Max-Planck-Institut f. Astrophysik and the observatory in Ondřejov for their hospitality during her successive stays. We thank the VTT staff and particularly Dr. Nicole Mein who processed the MSDP data and Dr. Art Poland who read and corrected the manuscript.

References

Aulanier, G., Démoulin, P.: 1998, *Astron. Astrophys.* **329**, 1125.
Aulanier, G., Démoulin, P.: 2003, *Astron. Astrophys.* **402**, 769.
Aulanier, G., Schmieder, B.: 2002, *Astron. Astrophys.* **386**, 1106.
Heinzel, P., Anzer, U.: 2001, *Astron. Astrophys.* **375**, 1082.
Heinzel, P., Anzer, U.: 2006, *Astrophys. J.* **643**, L65.
Heinzel, P., Anzer, U., Gunár, S.: 2005, *Astron. Astrophys.* **442**, 331.
Heinzel, P., Schmieder, B., Vial, J.C.: 1997, *Proc. SOHO 5 Workshop, ESA*, **SP-404**, 427.
Heinzel, P., Schmieder, B., Vial, J.C., Kotrč, P.: 2001, *Astron. Astrophys.* **370**, 281.
Karpen, J.T., Antiochos, S.K., Klimchuk, J.A.: 2006, *Astrophys. J.* **637**, 531.
Kippenhahn, R., Schlüter, A.: 1957, *Z. Astrophys.* **43**, 36.
Kuperus, M., Raadu, M.A.: 1974, *Astron. Astrophys.* **31**, 189.
Leroy, J.L., Bommier, V., Sahal-Bréchot, S.: 1984, *Astron. Astrophys.* **131**, 33.
Lin, Y.: 2002, *Solar Variability: From Core to Outer Frontiers, ESA*, **SP 506**, 681.
Litvinenko, Y.E., Martin, S.F.: 1999, *Solar Phys.* **190**, 45.
Martin, S.F.: 1998, *Solar Phys.* **182**, 107.
Mein, P.: 2002, *Astron. Astrophys.* **381**, 271.
Poland, A.I., Mariska, J.T.: 1986, *Solar Phys.* **104**, 303.
Poland, A.I., Mariska, J.T.: 1988, In: Ballester, J.L., Priest, E.R. (eds.) *Dynamics and Structure of Solar Prominences*, Universitat de les Illes Balears, Palma de Mallorca, p. 133.
Régnier, S., Amari, T.: 2004, *Astron. Astrophys.* **425**, 345.
Schmieder, B., Tziotziou, K., Heinzel, P.: 2003, *Astron. Astrophys.* **401**, 361.
Schmieder, B., Heinzel, P., Kucera, T., Vial, J.C.: 1998, *Solar Phys.* **181**, 309.
van Ballegooijen, A.: 2004, *Astrophys. J.* **612**, 519.
Wilhelm, K., Curdt, W., Marsch, E., *et al.*: 1995, *Solar Phys.* **162**, 189.